OPEN ACCESS
Functional Materials Letters
Vol. 14, No. 4 (2021) 2150008 (5 pages)

DOI: 10.1142/S1793604721500089

World Scientific
www.worldscientific.com

Structural and optical properties of ionic liquid-based hybrid perovskitoid: A combined experimental and theoretical investigation

Sachin Thawarkar*, Sachin R. Rondiya†, Prem Jyoti Singh Rana*, Ramanuj Narayan*, Nelson Y. Dzade† and Surya Prakash Singh*,‡

*Polymer and Functional Materials Division
CSIR-Indian Institute of Chemical Technology (IICT)
Uppal Road, Tarnaka, Hyderabad 500007, India
†School of Chemistry, Cardiff University
Main Building, Park Place, Cardiff
CF 10 3AT, Wales, UK
‡spsingh@iict.res.in

Received 29 December 2020; Accepted 12 February 2021; Published 27 April 2021

Herein, we report a novel layered lead bromide, $(CH_3CH_2)_3N^+Br^-(CH_2)_2NH_3^+)PbBr_3$, where bulky organic cations, $(CH_3CH_2)_3N^+Br^-(CH_2)_2NH_3^+)$, amino-ethyl triethyl ammonium [aetriea] were not only incorporated between the inorganic layers but also sandwiched within the inorganic $[PbBr_6]^{4-}$ octahedral layered structure. The UV-Visible, photoluminescence spectroscopy (PL), X-ray diffraction (XRD) and a field-emission scanning electron microscope (FE-SEM) result show that the new perovskitoid has a microrod shape with an estimated bandgap of ~3.05 eV. The structural and optoelectronic properties of the [aetriea]$PbBr_3$ perovskitoid were further corroborated by first-principles density functional theory (DFT) calculations. Thermogravimetric analysis (TGA) data show good stability of the [aetriea]$PbBr_3$ perovskitoid. Time-resolved photoluminescence (TRPL) decays from new [aetriea]$PbBr_3$perovskitoid showing 6 ns average lifetime. These results suggest that doubly charged cation hybrid perovskite materials are potential candidates for optoelectronic applications.

Keywords: Semiconductor; colloidal synthesis; crystal structure; optical properties; perovskitoid; DFT.

Hybrid perovskite (HP) materials have attracted significant attention in the scientific community due to their high efficiency of 25.5% in a short period of one decade.[1–4] HP possess outstanding optical properties such as large absorption coefficient, appropriate direct bandgap, high charge carrier mobility and low exciton binding energy for next-generation thin-film solar cell applications.[5,6] HP are attractive candidates for optoelectronic applications as they display excellent performance in light-emitting diodes, lasers, photodetectors and sensors.[7–13] However, the intrinsic instability and toxicity of HP materials limit their large-scale applications and commercialization.

The quest to improve the stability of hybrid perovskites has led to a significant number of investigations looking at other organic cations apart from the conventional methylammonium. It is possible to form low-dimensional (2D sheets, 1D chains and 0D clusters) organic–inorganic hybrid perovskitoid structures when larger organic ligands are used.[14,15] By incorporating other functional organic ligands, the properties of the resulting hybrid perovskitoid can be improved. For instance, the placement of MA/FA cation by larger organic cation such as phenethylammonium (PEA) cation in halide perovskites, resulted in the formation of 2D perovskitoids, which exhibit improved stability and moisture resistance comparedto the 3D counterparts.[16,17] The demonstrated enhancement of both the photostability and performance of layered hybrid perovskitoids[16,17] opened a new path for the investigation of novel solar cell absorbers. Generally, hybrid perovskitoid with alkylammonium derivatives organic cations shows large bandgap.[7,18] Ionic liquids (IL) are also attractive organic cations for the synthesis of stable perovskitoids owing to their unique physicochemical properties such as high electrical conductivity, high thermal stability, low vapor pressure and crystalline structure.[19–21]

Herein, we report to the synthesis of ionic liquid-based lead halide perovskitoid with the chemical formula $[(CH_3CH_2)_3N^+Br^-(CH_2)_2NH_3^+)]PbBr_3$ where the IL cations are integrated with an inorganic framework of infinite order of face sharing $[PbBr_6]^{4-}$ octahedral *via* anti-solvent

‡Corresponding author.

precipitation method. The structure, morphology, and optoelectronic properties of the as-prepared [aetriea]$PbBr_3$ NCs were comprehensively characterized using a range experimteal characterization techuniques (X-ray diffraction (XRD), Field Emission Scanning Electron Microscope (FE-SEM), UV-Visible and photoluminescence spectroscopy) and corroborated with DFT calculations.

Synthesis of perovskitoid [aetriea]$PbBr_3$ microcrystals: Hybrid organic–inorganic perovskitoid amino-ethyl triethyl ammonium lead bromide [aetriea]$PbBr_3$ perovskitoid was synthesized by antisolvent precipitation method. A mixture of 100 μL dimethyl sulfoxide (DMSO) and 10 mL dry toluene was made by stirring under nitrogen atmosphere. A precursor solution was prepared by mixing 0.16 mmol of [aetma] Br with 0.2 mmol of $PbBr_2$ with 20 μL oleylamine and 0.5 mL oleic acid in 5 mL DMF. Afterwards, 0.2 mL of the precursor solution was rapidly added into the toluene/DMF mixture, and stirring of the solution was stopped. The mixture was then kept at room temperature for 2 min and cooled for 10 min in an ice bath. The reaction solution was kept overnight for the precipitation of [aetriea]$PbBr_3$ perovskitoid. The [aetriea]$PbBr_3$ with different halide concentration was synthesized by mixing the preferred quantity of the halide precursor solutions according to Scheme S1 in Supporting Information.

DFT simulations: The first-principles density functional throery (DFT) calculations were performed using the Vienna Ab initio Simulation Package (VASP),[22–24] using generalized gradient approximation (GGA) and the Perdew–Burke–Ernzerhof (PBE) exchange-correlation functional. The interactions between the core and valence elections were described using the project augmented wave (PAW) method.[25] A Monkhorst-Pack[26] k-point mesh of $5 \times 5 \times 3$ was used for geometry optimization of the [aetriea]$PbBr_3$ perovskitoid, while a higher k-point mesh of $7 \times 7 \times 5$ was used for electronic structure calculations. The cut-off energy for the plane wave functions is set to 600 eV and the threshold of the total energy change is set to 10^{-6} eV. Geometry optimizations were performed using the conjugate-gradient algorithm until the residual Hellmann-Feynman forces on all relaxed atoms reached 10^{-3} eV Å^{-1}. Due to the strong relativistic correction on heavy Pb atoms, the spin-orbit coupling (SOC) was accounted for in calculations.[27,28] For accurate prediction of the bandgap [aetriea]$PbBr_3$ perovskitoid, the screened hybrid functional HSE06[29] was used with the exchange value of 25%. The projected density of states (PDOS) was calculated using the tetrahedron method with Bloch correction.[30] The optical properties of [aetriea]$PbBr_3$ was determined from the complex dielectric function, $\varepsilon(\omega) = \varepsilon_1(\omega) + i\,\varepsilon_2(\omega)$ within the independent-particle formalism.[31]

XRD analysis (Figure 1a) was carried out to ascertain the structure of the as-synthesized [aetriea]$PbBr_3$ perovskitoid thin film, deposited on a glass substrate. The XRD pattern reveals that all peaks can be indexed to the pure perovskitoid crystalline phase. The presence of multiple peaks in the XRD pattern confirms the poly-crystalline nature of the [aetriea]$PbBr_3$ thin film. The measured diffraction peak positions at 10.46°, 18.03°, 20.61°, 30.17°, 37.15°, 41.43°, 45.60° and 52.32° were converted into interplanar d-spacings of 0.84, 0.49, 0.43, 0.29, 0.24, 0.22, 0.19 and 0.17 nm, respectively. The peak intensity of the perovskitoid materials was significantly high and the full width at half-maximum (FWHM) is narrow as shown in Figs. 1(a) and S1, Supporting Information. This indicates that the crystallinity of our perovskitoid material is good, which leads to good optical properties. The obtained high-quality microrod perovskitoid nanocrystals have the potential to improve charge carrier separation and minimize recombination rates. The average crystallite size (D) of perovskitoid NCs can be determined from the full width at half maximum of the XRD peak using Scherrer's equation[32,33]:

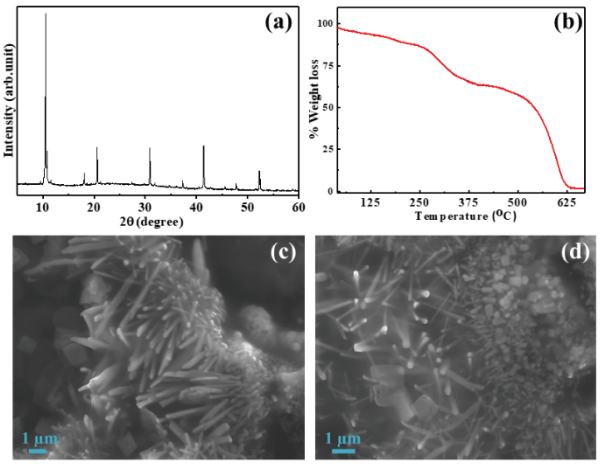

Fig. 1. (a) Thin film XRD pattern, (b) TGA curve, (c) and (d) FE-SEM images of [aetriea]$PbBr_3$ perovskitoid nanocrystals.

$$D = \frac{k\alpha}{\beta \cos\theta}, \tag{1}$$

where λ = 1.54 Å (X-ray diffractometer with Cu Kα radiation), β is the observed FWHM, θ is the diffraction angle of the peak 10.46° and k is a shape factor with a value of 1 for perovskitoid materials.

To understand the thermal stability of the as-synthesized [aetriea]$PbBr_3$ perovskitoid, we performed thermogravimetric analysis. The thermogravimetric analysis curve in Fig. 1(b) shows that there is no huge mass loss below 250 °C, demonstrating good thermal stability of the [aetriea]$PbBr_3$ perovskitoid NCs. The mass loss above 250 °C can be attributed to the degradation of organic ionic liquid cation and dehalogenation, whereas the mass loss between 500 °C to 600 °C is related to the degradation of lead bromide.

FE-SEM analysis is carried out to determine the morphology of the [aetriea]$PbBr_3$ perovskitoid. The FE-SEM images in Figs. 1(c) and 1(d) show that the [aetriea]$PbBr_3$ crystals have microrod-like shapes. In contrast, cubic morphologies have been reported for organic cation-based perovskite NCs.[34,35] The observed microrods shapes for the ILPbBr_3 perovskitoid may be due to the large and double-charged state of the IL cation compared to other cations, which have single charge and are small in size. The interactions between organic cations with doubly charged and bulky nature and inorganic anions $[PbBr_6]^{4-}$ may be different from the single charged and small size cations. These interactions may be responsible for change in the morphology of [aetriea]$PbBr_3$ perovskitoid as microrod shape.

The formation of the [aetriea]$PbBr_3$ nanocrystals perovskitoid was analyzed via several characterization techniques. The recorded UV-Visible [Figure 2(a)] and PL [Figure 2(c)] spectra both confirm the successful formation of the [aetriea]$PbBr_3$ nanocrystals perovskitoid. The sharp UV-Visible absorption peak is observed at 397 nm, whereas the PL spectrum is observed at 414 nm with excitation wavelength 370 nm. It is found that the optical absorption band and emission band are blue-shifted for [aetriea]$PbBr_3$ relative to other organic–inorganic hybrid perovskitoid. We have calculated the optical band gap for [aetriea]$PbBr_3$ perovskitoid nanocrystals from the absorption spectrum by *Tauc* plot and it is 3.05 eV, as shown in Fig. 2(b). The broadening of the bandgap is probably due to the result of an electrostatic and orientational disorder in the [aetriea]$PbBr_3$ crystals and enhanced exciton confinement by the incorporated IL ligand. To get further insights into the luminescence properties of the [aetriea]$PbBr_3$ perovskitoid NCs, we have recorded the time-resolved photoluminescence (TRPL) emission spectra.

Table 1. Photophysical data of [aetriea]$PbBr_3$ perovskitoid microrods.

NCs	τ_1 (ns)	α_1 (%)	τ_2 (ns)	α_2 (%)	CHI SQ	τ_{ave} (ns)
[aetriea]$PbBr_3$	2.06	50.80	8.26	49.20	1.47	5.94

Figure 2(d) displays the fitted TRPL spectra of [aetriea]$PbBr_3$ in toluene with excitation wavelength at 414 nm. The obtained decay pattern of the [aetriea]$PbBr_3$ perovskitoid NCs is fitted by using a multi-exponential function. The estimated kinetic parameters are given in Table 1. The average lifetimes of the ILPbBr_3 perovskitoid microrods were approximately 6 ns. The PL decay time of [aetriea]$PbBr_3$ perovskitoid NCs is reduced as compared to other hybrid organic–inorganic perovskitoid materials, which indicates that it enhances the nonradiative recombination rate.[36] This effect may be observed for the enhancement of surface defect density, which is increased may be due to more charge available on the organic ligands. The longer nonradiative recombination time indicates less energy loss, which genereally leads to better performance of solar cell.[37–39] However, more investigation is necessary to get additional insights into the phenomenon of exciton dynamics.

The [aetriea]$PbBr_3$ was modeled in the orthorhombic crystal structure Figs. 3(a) and 3(b), adopted also by $PEAPbI_3$.[40] Full geometry optimization of the two-dimensional [aetriea]$PbBr_3$ perovskitoid gave rise to the unit cell parameters: a = 7.692 Å, b = 7.727 Å and c = 20.524 Å. The calculated electronic band structure with the corresponding projected density of state are shown in Fig. 4. Analysis of the projected density of states reveals that the valence band edge is dominated by N p-states. The IL ligand introduces intermediate states near the conduction edge with the C p-states dominating. Relative to

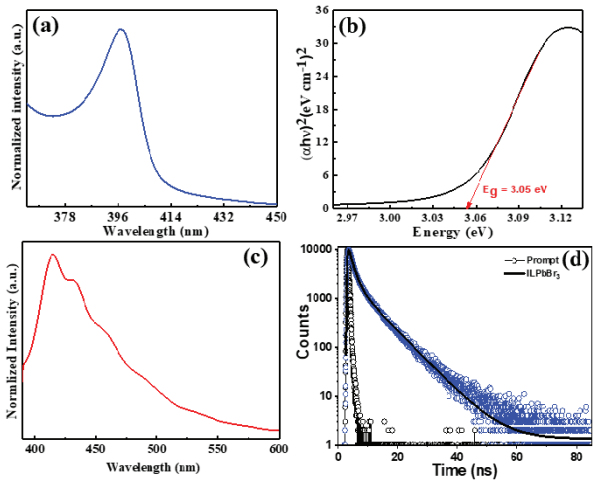

Fig. 2. (a) UV-Visible spectra, (b) *Tauc* plot for bandgap calculation, (c) PL of spectra and (d) Time-resolved PL decays for [aetriea]$PbBr_3$ perovskitoid nanocrystals in toluene.

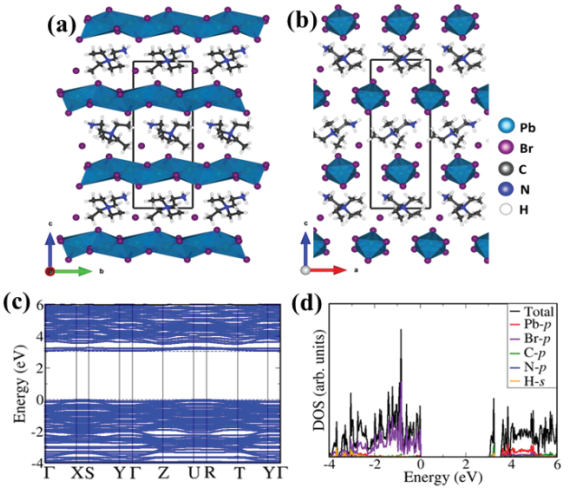

Fig. 3. (a) and (b) Polyhedral representation of ILPbBr3 (IL = $(CH_3CH_2)_3N^+Br^-(CH_2)_2NH_3^+$), (c) electronic band structure, and (d) partial density of states calculated for ILPbBr_3.

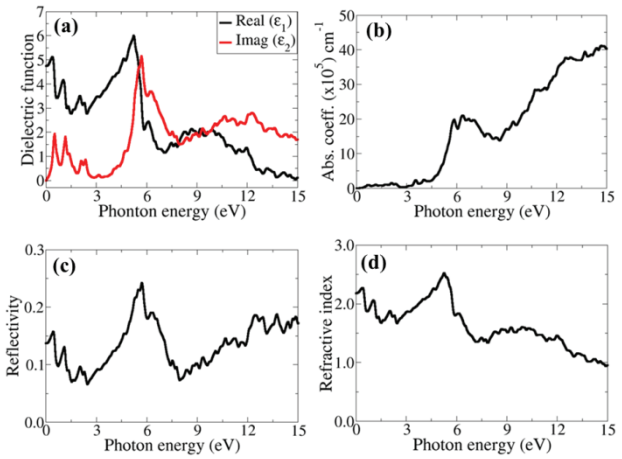

Fig. 4. Calculated (a) dielectric function, (b) absorbance, (c) reflectivity and (d) refractive index of [aetriea]$PbBr_3$.

the intermediate bands, the bandgap of the [aetriea]$PbBr_3$ perovskitoid is predicted at 3.10 eV, in close agreement with the experimental estimate of 3.05 eV from *Tauc* plot. Figure 3(a) shows layered structure of [aetriea]$PbBr_3$ perovskitoid, in which an organic cation is not only incorporated within the $[PbBr_6]^{4-}$ layered anion structure but it is also sandwiched between the inorganic perovskitoid layers. The calculated real (ε_1) and imaginary (ε_2) parts of the dielectric function for the [aetriea]$PbBr_3$ are shown in Fig. 4(a), with the dielectric constant predicted at 4.76. Negligible absorption occurs until after 3.0 eV, which is close to the fundamental bandgap.

The predicted high absorption coefficient after 3.0 eV in the order of 10^5 cm^{-1} makes [aetriea]$PbBr_3$ an attractive absorber for the photovoltaic application. Shown in Figs. 4(c) and 4(d) are the calculated reflectivity and refractive indeces, which are two important parameters necessary for solar applications. Whiles the reflectivity gives a measure of reflecting light or radiation, the refractive index, on the other hand, shows its transparency. The optical reflectivity of [aetriea]$PbBr_3$ starts at about13.7% and reaches a maximum value of 24% at an energy of 5.72 eV. The refractive index is predicted at 2.28 [Figure 4(d)], which is lower than that of Si ($\eta = 3.4$ at 550 nm).[41]

In summary, we have revealed a facile synthesis of two-dimensional hybrid [aetriea]$PbBr_3$ perovskitoid NCs at room temperature *via* anti-solvent method in single step of mixing of stoichiometric of lead tri-bromide and ionic liquids in DMF. The formation of the [aetriea]$PbBr_3$ perovskitoid microrods is confirmed by UV, PL spectroscopy and XRD analyses. The [aetriea]$PbBr_3$ perovskitoid displays well-defined microrods shape with an estimated bandgap of approximately 3.05 eV as confirmed by experimental and first-principles DFT characterization. TGA analysis shows that the new organic ligand is thermally stable up to 290 °C, suggesting its potential suitability for low-cost thin-film solar cell. Time-resolved photoluminescence studies have been carried out to understand the charge transfer dynamics in the [aetriea]$PbBr_3$ perovskitoid and it is shows anaverage of 6 ns lifetime. The successful synthesis and characterization of ionic liquid-based lead halide perovskitoid NCs should open the way to a new class of layered hybrid perovskitoid solar-cell absorbers.

Acknowledgments

ST is thankful to DST-SERB, NPDF award (No. PDF/2017/001668. SPS and RN acknowledge for all the support through in-house project funding, infrastructure and characterization facility. SPS thanks DST for Indo-Poland project DST/INT/POL/P-26/2016. SRR and NYD acknowledge the UK Engineering and Physical Sciences Research Council (EPSRC) for funding (Grant No. EP/S001395/1). This work has also used the computational facilities of the Advanced Research Computing at Cardiff (ARCCA) Division, Cardiff University and HPC Wales. This work also made use of the facilities of ARCHER (http://www.archer.ac.uk), the UK's national supercomputing service via the membership of the UK's HEC Materials Chemistry Consortium, which is funded by EPSRC (EP/L000202).

Information on the data that underpins the results presented here, including how to access them, can be found in the Cardiff University data catalogue at http://doi.org/10.17035/d.2021.0132065524.

References

1. B. Saparov and D. B. Mitzi, *Chem. Rev.* **116,** 4558 (2016).
2. Y. Zhong, R. Munir, J. Li, M.-C. Tang, M. R. Niazi, K. Zhao A. Amassian, *ACS Energy Lett.* **3**, 1078 (2018).
3. J. S. Manser, J. A. Christians and P. V. Kamat, *Chem. Rev.* **116** 12956 (2016).
4. K. P. Ong, T.W. Goh, Q. Xu and A. Huan, *J. Phys. Chem. A* **119**, 11033 (2015).
5. M. Saliba, T. Matsui, J.-Y. Seo, K. Domanski, J.-P. Correa-Baena, M. K. Nazeeruddin, S. M. Zakeeruddin, W. Tress, A. Abate, A. Hagfeldt and M. Grätzel, *Energy Environ. Sci.* **9**, 1989 (2016).
6. N. J. Jeon, J. H. Noh, W. S. Yang, Y. C. Kim, S. Ryu, J. Seo and S. I. Seok, *Nature* **517**, 476 (2015) .
7. J. Yu, M. Wang and S. Lin, *ACS Nano.* **10**, 11044 (2016).
8. Y. Zhou, X. Guan, H. Zhou, K. Ramadoss, S. Adam, H. Liu, S. Lee, J. Shi, M. Tsuchiya, D. D. Fong and S. Ramanathan, *Nature* **534**, 231 (2016).
9. J. Shi, X. Xu, D. Li and Q. Meng, *Small*. **11**, 2472 (2015).
10. Y. Wang, Y. Zhang, Y. Lu, W. Xu, H. Mu, C. Chen, H. Qiao, J. Song, S. Li, B. Sun, Y.-B. Cheng and Q. Bao, *Adv. Opt. Mater.* **3**, 1389 (2015).
11. F. Li, C. Ma, H. Wang, W. Hu, W. Yu, A. D. Sheikh and T. Wu, *Nat. Commun.* **6**, 8238 (2015).

12. H. J. Snaith *et al., Adv. Mater.* **28**, 923 (2016).
13. N. Marchal *et al*., *Chem. Mater.* **31**, 6880 (2019).
14. J. Shamsi, A. S. Urban, M. Imran, L. De Trizio and L. Manna, *Chem. Rev.* **119**, 3296 (2019).
15. A. M. Ganose, C. N. Savory and D. O. Scanlon, *Chem. Commun.* **53**, 20 (2017).
16. D. V. Mitzi, K. Chondroudis and C. R. Kagan, *Inorg. Chem.* **38**, 6246 (1999).
17. W. T. M. Van Gompel, R. Herckens, K. Hecke, B. Ruttens, J. D'Haen, L. Lutsen and D. Vanderzande, *Chem. NanoMat*. **5**, 323 (2019); J. V. Passarelli, D. J. Fairfield, N. A. Sather, M. P. Hendricks, H. Sai, C. L. Stern and S. M. Stupp, *J. Am. Chem. Soc*. **140**(23), 7313 (2018).
18. L. A. Muscarella, D. Petrova, R. Jorge Cervasio, A. Farawar, O. Lugier, C. McLure, M. J. Slaman, J. Wang, B. Ehrler, E. von Hauff and R. M. Williams, *ACS Appl. Mater. Interfaces.* **11**, 17555 (2019).
19. M. Amde, J.-F. Liu and L. Pang, *Environ. Sci. Technol*. **49**, 12611 (2015).
20. G. Velpula, R. Phillipson, J. X. Lian, D. Cornil, P. Walke, K. Verguts, S. Brems, H. Uji-i, S. De Gendt, D. Beljonne, R. Lazzaroni, K. S. Mali and S. De Feyter, *ACS Nano.* **13**, 3512 (2019).
21. Y. Zhou and J. Qu, *ACS Appl. Mater. Interfaces* **9**, 3209 (2017).
22. G. Kresse and J. Hafner, *Phys. Rev. B* **47**, 558 (1993).
23. G. Kresse and D. Joubert, *Phys. Rev. B* **59**, 1758 (1999).
24. G. Kresse and J. Furthmüller, *Phys. Rev. B* **54**, 11169 (1996).
25. P. E. Blöchl, *Phys. Rev. B.* **50**, 17953 (1994).
26. H. J. Monkhorst and J. D. Pack, *Phys. Rev. B* **13**, 5188 (1976).
27. I. E. Castelli, J. M. García-Lastra, K. S. Thygesen and K. W. Jacobsen, *APL Mater.* **2**, 081514 (2014).
28. A. Amat, E. Mosconi, E. Ronca, C. Quarti, P. Umari, Md. K. Nazeeruddin, M. Grätzel and F. De Angelis, *Nano Lett.* **14**, 3608 (2014).
29. A. V. Krukau, O. A. Vydrov, A. F. Izmaylov and G. E. Scuseria, *J. Chem. Phys.***125**, 224106 (2006).
30. P. E. Blöchl, O. Jepsen and O. K. Andersen, *Phys. Rev. B* **49**, 16223 (1994).
31. E. Belarbi, M. Vallés-Pelarda, B. Clasen Hames, R. S. Sanchez, E. M. Barea, H. Maghraoui-Meherzi and I. Mora-Seró, *Phys. Chem. Chem. Phys.***19**, 10913 (2017).
32. S. Thawarkar, P. J. S. Rana, R. Narayan and S. P. Singh, *Langmu*ir. **35**, 17150 (2019).
33. A. R. West, *Solid State Chemistry and Its Applications* (Wiley, New York, 1974).
34. Y. Li, J. F. Galisteo-López, M. E. Calvo andH. Míguez, *ACS Appl. Mater. Interfaces* **9**, 35505 (2017).
35. C. A. López, M. V. Martínez-Huerta, M. C. Alvarez-Galván, P. Kayser, P. Gant, A. Castellanos-Gomez, M. T. Fernández-Díaz, F. Fauth and J. A. Alonso, *Inorg. Chem.* **56**, 14214 (2017).
36. J. Liu and O. V. Prezhdo, *J. Phys. Chem. Lett.* **6**, 4463 (2015).
37. L. Qiao, W.-H. Fang and R. Long, *J. Phys. Chem. Lett.* **10**, 7237 (2019).
38. S. Thawarkar, S. Rondiya, N. Dazade, N. Khupse and S. Jadkar, *Chem. Eur. J*. **27**, 1 (2021).
39. S. S. Mali, J. V. Patil, J. A. Steele, S. R. Rondiya, N. Y. Dzade and C. K. Hong, *ACS Energy Lett*. **6**, 778 (2021).
40. C. Chen, L. Gao, W. Gao, C. Ge, X. Du, Z. Li, Y. Yang, G. Niu and J. Tang, *Nat Commun.* **10**, 1927 (2019).
41. W. Primak, *Appl. Opt.* **10**, 759 (1971).